J. Fluid Mech. (2006), *vol.* 560, *pp.* 1–17.
doi:10.1017/S0022112006000462 Printed in the United Kingdom

The stability of a quasi-geostrophic ellipsoidal vortex in a background shear flow

By WILLIAM J. McKIVER AND DAVID G. DRITSCHEL

School of Mathematics and Statistics, University of St Andrews, St Andrews, UK

(Received 17 September 2005 and in revised form 6 January 2006)

We consider the motion of a single quasi-geostrophic ellipsoid of uniform potential vorticity in equilibrium with a linear background shear flow. This motion depends on four parameters: the height-to-width aspect ratio of the vortex, h/r, and three parameters characterizing the background shear flow, namely the strain rate, γ, the ratio of the background rotation rate to the strain, β, and the angle from which the shear is applied, θ. We generate the equilibria over a large range of these parameters and analyse their linear stability. For the second-order ($m = 2$) modes which preserve the ellipsoidal form, we are able to derive equations for the eigenmodes and growth rates. For the higher-order modes we use a numerical method to determine the full linear stability to general disturbances ($m > 2$).

Overall we find that the equilibria are stable over most of the parameter space considered, and where instability does occur the marginal instability is usually ellipsoidal. From these results, we determine the parameter values for which the vortex is most stable, and conjecture that these are the vortex characteristics which would be the most commonly observed in turbulent flows.

1. Introduction

Observations of the Earth's atmosphere and oceans reveal a great number of vortices at many different scales (Holton *et al.* 1995; Ebbesmeyer *et al.* 1986). These vortices, or coherent regions of anomalous potential vorticity, interact in a variety of ways, ranging from quasi-steady behaviour where the vortex only weakly feels the effects of its surroundings, to strong turbulent interactions where vortices can merge, split and filament. Despite their complicated interactions many vortices have a relatively long lifespan, for example the Mediterranean salt lenses (Meddies) which have been observed in many studies (Armi *et al.* 1989). These observations indicate that certain vortices are highly stable to the effects of their surroundings. This has fuelled an interest in the idealized problem of a single vortex subjected to the effects of a background flow. This background flow, taken to be linear in spatial coordinates, approximates the leading-order influence of surrounding vortices.

Initially this problem was considered only for the two-dimensional case of an elliptical patch of constant vorticity (Kida 1981; Dritschel 1990). More recently Zhmur & Shchepetkin (1991) and Meacham (1992) extended this problem to the three-dimensional rotating stratified case where they studied an ellipsoidal vortex within the quasi-geostrophic model. Meacham (1992) studied the stability of a freely rotating ellipsoid of potential vorticity (PV) and found instabilities over a large range of the parameter space characterizing the ellipsoid. However, recently Dritschel, Scott & Reinaud (2005) have found that one of the unstable modes Meacham encountered

is in fact stable, and overall their results indicate that the freely rotating ellipsoid is widely stable. Miyazaki, Ueno & Shimonishi (1999) studied the stability of a spheroid of uniform PV tilted by some inclination angle from the vertical axis. They found that highly prolate spheroids are unstable if the inclination angle is large, while oblate spheroids are unstable even if the inclination angle is very small. In both cases the instability is non-ellipsoidal, i.e. it destroys the ellipsoidal form of the vortex. Hashimoto, Shimonishi & Miyazaki (1999) derived the equations for the linear stability of an ellipsoid in a two-dimensional strain field, and using these they studied the cases of a pure strain field (when there is no background rotation) and a simple shear flow (when the strain rate is equal to the background rotation). They found that in a pure strain field, highly elongated ellipsoids are unstable to modes whose order m is greater than 2, i.e. to non-ellipsoidal modes. In a simple shear flow they found that a highly elongated ellipsoid whose major axis is perpendicular to the flow direction is unstable, whereas any ellipsoidal vortex seems to be stable if the major axis is parallel to the flow direction. Meacham *et al.* (1994) derived equations for the evolution of an ellipsoid of uniform PV in a background flow with both horizontal strain and vertical shear. They examined the stability for some special background flows, either pure horizontal strain or pure vertical shear (in the absence of horizontal strain).

To date, there has been no complete study of the combined effects of horizontal strain and vertical shear on an ellipsoid of uniform PV. In this paper we will examine this problem. The roots of our approach lie in a reformulation of the problem introduced by McKiver & Dritschel (2003). In this reformulation, the system depends on four parameters: the height-to-width aspect ratio of the vortex, h/r, and three parameters that specify the background flow. Reinaud, Dritschel & Koudella (2003) introduced a method for determining the steady equilibrium states for this system. They determined possible equilibria over a wide range of the parameters and found that vortices with aspect ratios of around $h/r = 0.8$ (in coordinates rescaled by f/N where f and N are the constant Coriolis and buoyancy frequencies respectively) are best able to survive the effects of the background flow. They also found $h/r = 0.8$ to be the most commonly observed aspect ratio in high-resolution turbulence simulations having large populations of vortices.

Here we will not only determine the steady states, but we will also analyse their linear stability to both ellipsoidal and non-ellipsoidal disturbances over a far greater range of the parameters than previously considered. In § 2 we present the equations of motion and describe the method for determining the steady states of this system, following Reinaud *et al.* (2003). In § 3.1 we derive the linear stability equations for the second-order modes, i.e. the purely ellipsoidal disturbances. In § 3.2 we review the method of Reinaud & Dritschel (2002) for analysing the full linear stability. In § 4 we present the results from both the ellipsoidal and full linear stability analyses. We conclude in § 5.

2. The model problem

2.1. *The quasi-geostrophic ellipsoid*

The quasi-geostrophic (QG) model is an approximate model of large-scale mid-latitude geophysical flows. It incorporates two important features underpinning these geophysical flows: the effects of the Earth's rotation and density stratification (lighter fluid lying on denser fluid). Here we consider the Coriolis frequency, f, and the buoyancy frequency, N, to be constant, allowing us to rescale the vertical coordinate

by Prandtl's ratio f/N. Then the QG equations can be written as

$$\frac{\mathrm{D}q}{\mathrm{D}t} = \frac{\partial q}{\partial t} + u\frac{\partial q}{\partial x} + v\frac{\partial q}{\partial y} = 0, \tag{2.1a}$$

$$\nabla^2\psi = q, \tag{2.1b}$$

$$\boldsymbol{u} = \mathscr{L}\nabla\psi, \tag{2.1c}$$

where q is the potential vorticity, ψ is the streamfunction, $\boldsymbol{u} = (u, v)$ is the horizontal velocity field and

$$\mathscr{L} = \begin{pmatrix} 0 & -1 & 0 \\ 1 & 0 & 0 \\ 0 & 0 & 0 \end{pmatrix}. \tag{2.2}$$

If we consider a uniform ellipsoid of PV placed at the origin, with semi-axis lengths a, b and c, each of which is directed along the unit vectors $\hat{\boldsymbol{a}}$, $\hat{\boldsymbol{b}}$ and $\hat{\boldsymbol{c}}$ respectively, and which is subjected to an external linear background flow of the form

$$\boldsymbol{u}_\mathrm{b}(\boldsymbol{x}, t) = \mathscr{S}_\mathrm{b}(t)\boldsymbol{x} \tag{2.3}$$

then it can be shown (McKiver & Dritschel 2003) that the evolution of the ellipsoid is governed by

$$\frac{\mathrm{d}\mathscr{B}}{\mathrm{d}t} = \mathscr{S}\mathscr{B} + \mathscr{B}\mathscr{S}^T, \tag{2.4}$$

where $\mathscr{B}$ and $\mathscr{S}$ are 3×3 matrices which we will refer to as the 'shape' matrix and the 'flow' matrix respectively. The shape matrix encapsulates the size and orientation of the ellipsoid and is given by

$$\mathscr{B} = a^2\hat{\boldsymbol{a}}\hat{\boldsymbol{a}}^T + b^2\hat{\boldsymbol{b}}\hat{\boldsymbol{b}}^T + c^2\hat{\boldsymbol{c}}\hat{\boldsymbol{c}}^T. \tag{2.5}$$

The flow matrix can be decomposed into two parts, $\mathscr{S} = \mathscr{S}_\mathrm{v} + \mathscr{S}_\mathrm{b}$, where $\mathscr{S}_\mathrm{v}$ is the self-induced part and $\mathscr{S}_\mathrm{b}$ is the part due to the linear background flow. $\mathscr{S}_\mathrm{v}$ is given by

$$\mathscr{S}_\mathrm{v} = \mathscr{L}\mathscr{P}_\mathrm{v} \tag{2.6}$$

where the 3×3 matrix $\mathscr{P}_\mathrm{v}$ is obtained by inverting the Laplacian in equation (2.1*b*) for the ellipsoid (a result found by Laplace 1784) and is

$$\mathscr{P}_\mathrm{v} = \xi_a\hat{\boldsymbol{a}}\hat{\boldsymbol{a}}^T + \xi_b\hat{\boldsymbol{b}}\hat{\boldsymbol{b}}^T + \xi_c\hat{\boldsymbol{c}}\hat{\boldsymbol{c}}^T \tag{2.7}$$

where

$$\xi_a = \kappa_v R_D(b^2, c^2, a^2), \tag{2.8a}$$

$$\xi_b = \kappa_v R_D(c^2, a^2, b^2), \tag{2.8b}$$

$$\xi_c = \kappa_v R_D(a^2, b^2, c^2). \tag{2.8c}$$

R_D is the elliptical integral of the second kind (see Appendix A) and $\kappa_v = \frac{4}{3}\pi abcq$ is the vortex 'strength'. We obtain the background flow matrix $\mathscr{S}_\mathrm{b}$ by Taylor expanding the streamfunction due to a distant vortex to second order giving us (McKiver & Dritschel 2003)

$$\mathscr{S}_\mathrm{b} = \gamma \begin{pmatrix} 0 & \frac{1}{2}(1 + 3\cos 2\theta) + \beta & \frac{3}{2}\sin 2\theta \\ 1 - \beta & 0 & 0 \\ 0 & 0 & 0 \end{pmatrix} \tag{2.9}$$

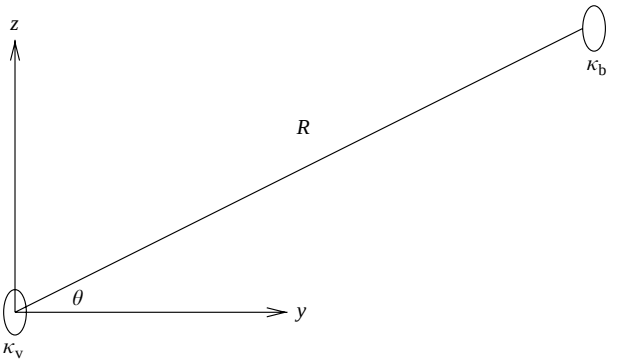

FIGURE 1. Schematic showing the vortex configuration.

where the strain rate is defined by

$$\gamma \equiv \kappa_b / R^3 \tag{2.10}$$

and β is the ratio of the background rotation rate to the strain rate, i.e.

$$\beta \equiv (\kappa_b + \kappa_v)/\kappa_b \tag{2.11}$$

where κ_b is the strength of the background vortex and R is the distance between the vortex centroids. The angle θ is defined such that the centroid of the background vortex is located at $(x, y, z) = (0, R\cos\theta, R\sin\theta)$ and ranges between 0° and 90° because of symmetry — see figure 1. Without loss of generality we set the PV, q, of the ellipsoid equal to unity in what follows. As noted in Reinaud *et al.* (2003), because $\kappa_v > 0$ when $\beta < 1$ we must have $\gamma < 0$; similarly when $\beta > 1$ we require $\gamma > 0$. These two cases correspond to opposite-signed and like-signed vortex interaction respectively. The case where $\beta \to 1$ implies $|\kappa_b/\kappa_v| \to \infty$, corresponding to the special cases of adverse shear for $\gamma > 0$ and cooperative shear for $\gamma < 0$. In all that follows when we examine the case $\beta = 1$, we take $\gamma > 0$, i.e. the case of adverse shear.

The full model is thus governed by the evolution equation (2.4), the self-induced flow matrix (2.6) and the background flow matrix (2.9). Owing to the lack of vertical advection, the height of the vortex is conserved. Also the volume is conserved because of incompressibility. Thus we can specify a particular vortex shape using its height-to-width aspect ratio, h/r, where h is the half-height of the vortex and r is effectively its mean radius. Thus our model depends on four parameters: h/r, β, θ and γ.

2.2. *The steady states*

The steady states for the ellipsoidal model are obtained by solving the following nonlinear system of equations:

$$\mathscr{S}\mathscr{B} + \mathscr{B}\mathscr{S}^T = 0. \tag{2.12}$$

Note that $\mathscr{S}$ depends on $\mathscr{B}$ through $\mathscr{S}_v$, defined in equation (2.6). Equation (2.12) is solved numerically using the iterative linear method described in Reinaud *et al.* (2003). This uses an initial guess for the $\mathscr{B}$ matrix (usually a known nearby equilibrium; for zero strain γ, $\mathscr{B}$ corresponds to a vortex with a circular cross-section and with its axes aligned with the coordinate axes) and then uses the linearized form of equation (2.12) to obtain the next iteration. Note that these equations cannot be inverted directly; instead one equation is removed and conservation of volume is enforced to close the equations (see Reinaud *et al.* 2003). The iterative process is repeated until

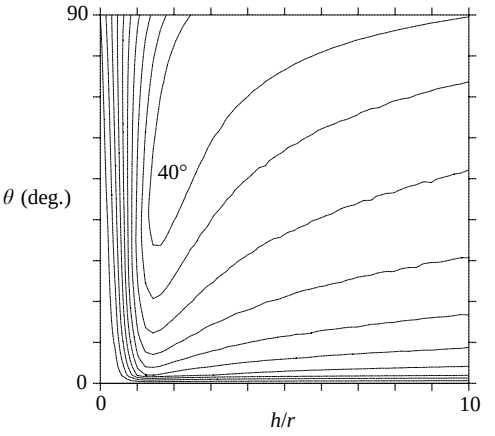

FIGURE 2. Contour maps of $\chi(h/r, \theta)$ for steady states at the turning point with $\beta = 1.0$. The minimum and maximum contour values displayed are 0° and 40° respectively, and the contour interval is 4°. The contour corresponding to $\chi = 0°$ lies along the axis $\theta = 0°$, and thus cannot be seen. The $\chi = 40°$ contour level is indicated.

the r.m.s. error, ΔB, between the five independent components of $\mathscr{B}$ at successive iterations is less than 10^{-10}. Since the volume and the half-height of the ellipsoid are conserved, the height-to-width aspect ratio h/r of the ellipsoid is unchanged throughout the procedure. Having thus found a solution, the strain $|\gamma|$ is increased by a small amount $|\mathrm{d}\gamma| = 10^{-4}$ and the procedure is repeated. If we find $\Delta B > 1$ or perform more than 10000 iterations, the procedure is stopped. When this occurs, we assume there is no steady state for the particular parameters considered.

For a given $(h/r, \beta, \theta)$, we have found steady states for values of γ up to a critical turning point, γ_c, i.e. the strain value beyond which there appear to be no more steady states. We consider both oblate and prolate vortices. For the oblate case, we examine the aspect ratios $h/r = k/10$, where $k = 1, 2, \ldots, 10$, and for the prolate case $h/r = 10/k$, where $k = 1, 2, \ldots, 9$. For each aspect ratio, we have considered both opposite-signed interactions for $-4 \leqslant \beta < 1$ and like-signed interactions for $1 \leqslant \beta \leqslant 6$. These values were chosen to be uniformly distributed in β with an increment $\Delta\beta = 0.2$. This represents a wide variation of the vortex strength ratio $\kappa_\mathrm{v}/\kappa_\mathrm{b}$. The case when there is no background flow corresponds to $|\beta| \to \infty$ and has already been studied by Meacham *et al.* (1992), Miyazaki *et al.* (1999) and Dritschel *et al.* (2005). For each value of β we consider $0° \leqslant \theta < 90°$ in increments of $\Delta\theta = 2°$. No deformation of the vortex occurs for $\theta = 90°$, as this corresponds to two vertically aligned vortices.

When $\gamma = 0$ the principal axes of the equilibrium vortices are aligned with the coordinate axes. As $|\gamma|$ increases, the axis originally aligned with the z-axis makes an angle χ with respect to that axis in the (y, z)-plane (no tilt into the (x, z)-plane ever occurs). In general the principle axes of the equilibrium vortices are either aligned with the coordinate axes, or are tilted about the x-axis by an angle, χ, with respect to the z-axis. In figure 2 we show $\chi(h/r, \theta)$ for the steady states at the turning point $\gamma = \gamma_c$ for the case $\beta = 1$. When $\theta = 0°$ the principle axes are aligned with the coordinate axes, i.e. $\chi = 0°$. For oblate vortices, $h/r < 1$, the tilt angle is small and does not vary much with θ. The tilt angle is also small for prolate vortices when θ is close to 0°, but increases sharply as θ increases. The figure confirms that prolate vortices are more sensitive to vertical shear than are oblate vortices. The latter tilt

only weakly with increasing θ. The decrease of χ for increasingly prolate vortices is due to weakening vertical shear at the turning point (see figure 7).

3. Linear stability analysis

Now we examine the stability properties of the steady states obtained. There are various orders of modes, $m = 0, 1, 2, \ldots$, which correspond to increasing orders of deformation. The zeroth-order mode corresponds to a change in volume, which is not allowed because of incompressibility. The $m = 1$ mode corresponds to the vortex being translated while preserving its shape and orientation, and thus cannot destabilize the vortex. The $m = 2$ mode corresponds to a change in vortex shape which preserves its ellipsoidal form, hence we refer to this as the ellipsoidal mode. For the ellipsoidal mode we will derive analytical equations for the growth rates. To obtain results for higher-order instabilities we use a numerical method described by Reinaud & Dritschel (2002).

3.1. *Ellipsoidal mode*

In order to examine the linear stability of ellipsoidal disturbances we linearize equation (2.4), writing the $\mathscr{B}$ matrix as follows:

$$\mathscr{B}(t) = \mathscr{B}_e + \mathscr{B}'(t), \tag{3.1}$$

where $\mathscr{B}_e$ is the equilibrium (steady-state) matrix and $\mathscr{B}'$ is an infinitesimal perturbation. Since $\mathscr{B}$ is a symmetric matrix, it has only six independent components, and it is convenient at this stage to introduce the following short-hand notation for the elements of $\mathscr{B}$:

$$\mathscr{B} = \begin{pmatrix} B^1 & B^2 & B^3 \\ B^2 & B^4 & B^5 \\ B^3 & B^5 & B^6 \end{pmatrix} = \sum_{k=1}^{6} \mathscr{J}^k B^k, \tag{3.2}$$

where the matrices $\mathscr{J}^k$ are

$$\mathscr{J}^1 = \begin{pmatrix} 1 & 0 & 0 \\ 0 & 0 & 0 \\ 0 & 0 & 0 \end{pmatrix}, \quad \mathscr{J}^2 = \begin{pmatrix} 0 & 1 & 0 \\ 1 & 0 & 0 \\ 0 & 0 & 0 \end{pmatrix}, \quad \mathscr{J}^3 = \begin{pmatrix} 0 & 0 & 1 \\ 0 & 0 & 0 \\ 1 & 0 & 0 \end{pmatrix}, \tag{3.3a}$$

$$\mathscr{J}^4 = \begin{pmatrix} 0 & 0 & 0 \\ 0 & 1 & 0 \\ 0 & 0 & 0 \end{pmatrix}, \quad \mathscr{J}^5 = \begin{pmatrix} 0 & 0 & 0 \\ 0 & 0 & 1 \\ 0 & 1 & 0 \end{pmatrix}, \quad \mathscr{J}^6 = \begin{pmatrix} 0 & 0 & 0 \\ 0 & 0 & 0 \\ 0 & 0 & 1 \end{pmatrix}. \tag{3.3b}$$

Using (3.2) and (3.3) we can write the Taylor expansion of the self-induced flow matrix about the equilibrium as

$$\mathscr{S}_{\mathrm{v}}(\mathscr{B}) = \mathscr{S}_{\mathrm{v}}(\mathscr{B}_e) + \sum_{k=1}^{5} B'^k \left. \frac{\partial \mathscr{S}_{\mathrm{v}}}{\partial B^k} \right|_{\mathscr{B}=\mathscr{B}_e}, \tag{3.4}$$

using (3.2) (recall $B'^6 = 0$ since there is no vertical motion). Taking $\mathscr{B}' = \hat{\mathscr{B}} \mathrm{e}^{\sigma t}$ and substituting (3.1) and (3.4) into (2.4) we obtain

$$\sum_{k=1}^{5} \mathscr{C}^k \hat{B}^k = \sigma \hat{\mathscr{B}}, \tag{3.5}$$

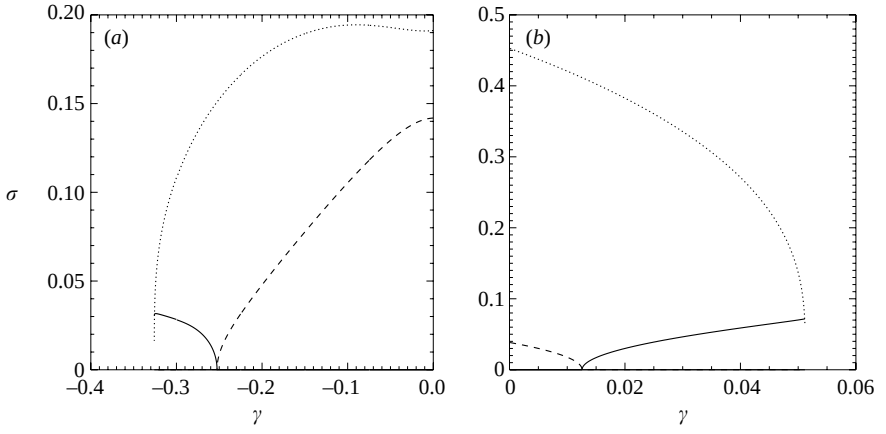

FIGURE 3. The frequencies σ_i and growth rates σ_r as a function of the strain rate γ for (*a*) $h/r = 0.6$, $\beta = 0.8$, $\theta = 70^\circ$ and (*b*) $h/r = 5.0$, $\beta = 1$, $\theta = 0^\circ$. The solid line and the dashed line correspond to the growth rate and the frequency for the M2(1) mode, respectively. The dotted line corresponds to the frequency of the M2(2) mode.

where

$$\mathscr{C}^k = \left.\frac{\partial \mathscr{S}_{\mathrm{v}}}{\partial B^k}\right|_{\mathscr{B}=\mathscr{B}_e} \mathscr{B}_e + \mathscr{S}\,\mathscr{J}^k + \mathscr{J}^k \mathscr{S}^T + \mathscr{B}_e \left.\frac{\partial \mathscr{S}_{\mathrm{v}}{}^T}{\partial B^k}\right|_{\mathscr{B}=\mathscr{B}_e}. \tag{3.6}$$

Note that the matrices, $\mathscr{C}^k$, can be determined using a known formula for the derivative of the self-induced flow matrix $\mathscr{S}_{\mathrm{v}}$ with respect to B^k (see Appendix B for details). Next we define the vector $\hat{\boldsymbol{B}} = (\hat{B}^1, \hat{B}^2, \hat{B}^3, \hat{B}^4, \hat{B}^5)$ and the 5×5 matrix $\boldsymbol{M}$ such that

$$M_{k1} = \mathscr{C}^k_{11}, \quad M_{k2} = \mathscr{C}^k_{12}, \quad M_{k3} = \mathscr{C}^k_{13,} \quad M_{k4} = \mathscr{C}^k_{22}, \quad M_{k5} = \mathscr{C}^k_{23}. \tag{3.7}$$

Using these we can rewrite (3.5) to obtain the eigenvalue problem

$$\boldsymbol{M}\hat{\boldsymbol{B}} = \sigma\,\hat{\boldsymbol{B}} \tag{3.8}$$

whose eigenvectors and eigenvalues correspond to the ellipsoidal disturbances and their growth rates. This eigenvalue problem can be solved using standard numerical methods. The equilibrium is unstable if there exists an eigenvalue σ with a positive real part, $\sigma_r > 0$, otherwise it is neutrally stable (all eigenmodes have $\sigma_r = 0$). Thus the real and imaginary parts of σ correspond to the growth rate and frequency respectively. In general the solutions are $\sigma = 0, \pm\sigma_{2(1)}, \pm\sigma_{2(2)}$ which correspond to the modes M2(0), M2(1) and M2(2) identified in Hashimoto *et al.* (1999) who considered a vortex in a horizontal strain ($\theta = 0^\circ$), but here we have generalized their results to the case of vertical shear. In figure 3 we plot the frequencies and the growth rates of the M2(1) modes and frequencies of the M2(2) modes for two cases. In both cases the M2(1) mode erupts before the turning point, whereas the M2(2) mode erupts at the turning point as indicated by its frequency going to zero as $\gamma \to \gamma_c$. This has been found for all the cases considered over the entire parameter space. Thus there is at most one unstable ellipsoidal mode which occurs before the turning point, namely the M2(1) mode.

3.2. *Full linear stability method*

For the full linear stability, i.e. for modes $m \geqslant 2$, we use a numerical method introduced by Reinaud & Dritschel (2002) for general three-dimensional QG equilibria. This method represents the equilibrium PV distribution by boundary contours in vertical layers. In our case the boundary contours are ellipses. The boundary of each contour is described by a horizontal position vector $\boldsymbol{x}_e(\phi) = (x_e, y_e)$ where ϕ is the travel time

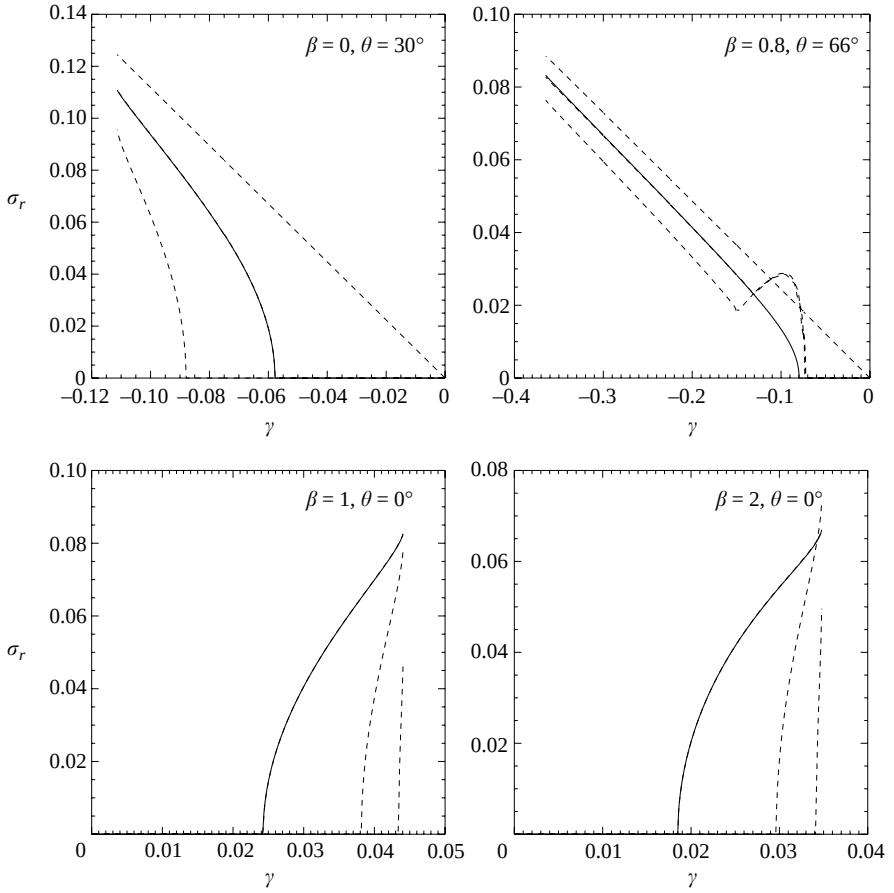

FIGURE 4. The growth rates σ_r as a function of the strain rate γ for $h/r = 2.5$ and a few different values of β and θ as indicated. The solid and dashed curves correspond to the ellipsoidal and non-ellipsoidal modes respectively. Note that the solid curve lies on top of one of the dashed curves in all cases.

coordinate, i.e. a quantity proportional to the time that it takes a fluid particle to travel along the equilibrium contour. The contour is perturbed by adding a perturbation, η, in the normal direction to the contour. The evolution equation of this perturbation can be obtained to first order (see Reinaud & Dritschel 2002) and by expanding the perturbation in terms of a truncated Fourier series expansion in ϕ multiplied by an exponential time factor, one can obtain the eigenvalue equation for the system.

For the results presented in § 4 we use $M = 5$ azimuthal modes and $n_c = 40$ contours, each of which is discretized into 120 points, connected by cubic splines. As found in many previous works, the stability results prove highly insensitive to doubling M, since the unstable modes (when they occur) are dominated by large-scale shape deformations. A detailed discussion of the accuracy of the method, including typical forms of the shape deformations, is given in Dritschel *et al.* (2005).

4. Stability results

From the ellipsoidal stability analysis, we know that there is at most one unstable mode before the turning point. For the full stability problem, we consider the three largest unstable modes (when there are any). In figure 4 we illustrate the growth

rates as a function of γ for $h/r = 2.5$ and a few different values of β and θ as indicated. The solid curve corresponds to the results of the purely ellipsoidal stability analysis whereas the dashed curves were obtained using the numerical method for the full stability. In the case of $\beta < 1$ (top two panels) there is a linear growth rate which corresponds to the centroid mode, i.e. to the ellipsoid being translated without deformation or change in orientation. As we do not consider this a real instability we have eliminated this mode from the results presented in the next section. The marginal instability is an ellipsoidal mode in each case except one, when $\beta = 0.8$ and $\theta = 66^\circ$ where the marginal instability is found to be a third-order non-ellipsoidal mode ($m = 3$).

4.1. *Opposite-signed interactions ($\beta < 1$)*

We first present the general stability results for opposite-signed vortices. In figure 5 we show contour maps of the magnitude of the strain rate found at the margin of stability of the ellipsoidal mode, $\gamma_e(\beta, \theta)$, the marginal non-ellipsoidal mode, $\gamma_n(\beta, \theta)$ (i.e. the higher-order mode with the smallest strain magnitude), and the turning-point strain rate, $\gamma_c(\beta, \theta)$, for several values of the aspect ratio, h/r. Here the bold, dashed and thin contours correspond to γ_e, γ_n and γ_c respectively. The contour interval is 0.01 and the minimum and maximum values plotted are 0.01 and 0.2.

From the contour plots we see that for the most oblate vortices ($h/r = 0.2$ and $h/r = 0.4$) there are no instabilities before the turning point. Ellipsoidal instability occurs for $h/r = 0.6$ for a small range of the parameter space but as h/r increases the range of this instability increases. Non-ellipsoidal instabilities also become more widespread with increasing aspect ratio, first occurring for $h/r = 0.8$; however over most of parameter space γ_n is greater than γ_e. Thus greater strain values are needed to induce non-ellipsoidal instabilities than ellipsoidal ones and so the marginal instability corresponds to the ellipsoidal mode. The gap between this marginal instability and the turning point increases with increasing aspect ratio h/r. Also the magnitude of this marginal strain, γ_m, increases as β approaches 1. Hence from the definition of β ($= 1 + \kappa_v/\kappa_b$), γ_m approaches a maximum as $|\kappa_b/\kappa_v| \to \infty$, which implies that *interactions between vortices of extremely different sizes are least destructive.*

From figure 5 we can also identify how the magnitude of the marginal strain, $\gamma_m = \gamma_e$, varies with the angle θ. For $h/r < 0.8$, γ_m increases with increasing θ, but for $h/r \geqslant 0.8$ it can be seen (cf. the troughs in the curves as a function of θ) that γ_m decreases for a range of θ values, but eventually reaches a maximum as $\theta \to 90^\circ$. The angle which corresponds to the minimum absolute value of γ_m will be referred to as θ_m. For $h/r < 1.0$, $\theta_m = 0^\circ$, whereas for $h/r \geqslant 1.0$, θ_m is between 55° and 75°, i.e. these are the most unstable angles. Because the strain is proportional to the inverse cube of the separation distances between two vortices, this implies that vortices with $h/r \geqslant 1.0$ which are vertically offset by an angle θ_m destabilize from the greatest separation distances. By contrast, oblate vortices with $h/r < 1.0$ destabilize from the greatest separation distance when they are vertically aligned ($\theta_m = 0$).

Figure 5 exhibits a kink in the turning-point strain contours. This kink is associated with a change in orientation of the ellipsoidal steady states as θ varies as can be seen in figure 6. This occurs when $\mathscr{B}_{11} = \mathscr{B}_{22}$, i.e. when two of the principal axes of the ellipsoid switch.

Finally by inspecting figure 5 we are able to see how the marginal strain values change with aspect ratio, h/r. Overall the largest strain values occur for aspect ratios between 1.0 and 1.25. Thus it appears that vortices having an aspect ratio close to

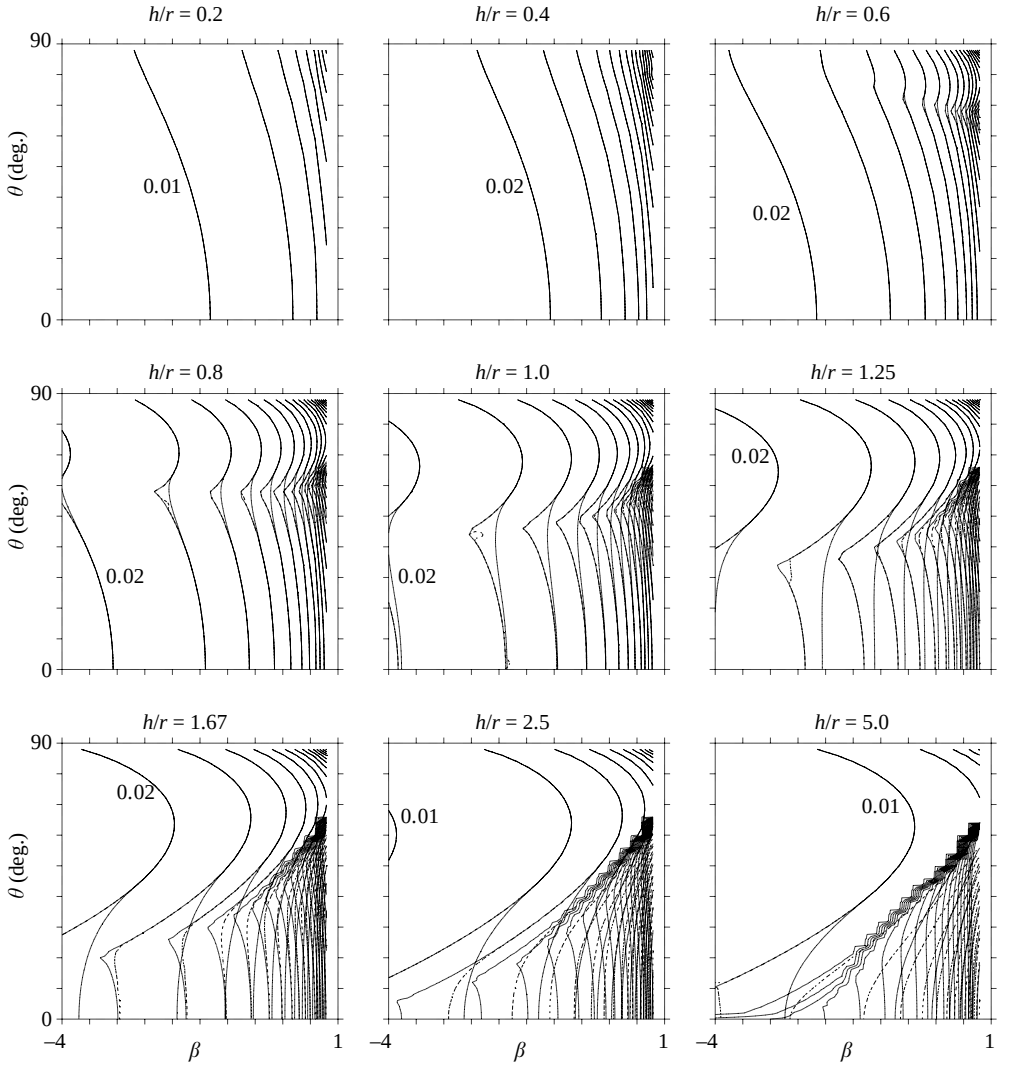

FIGURE 5. Contour maps of $|\gamma(\beta, \theta)|$ for various aspect ratios h/r for opposite-signed vortices ($\beta < 1$). The contour values with the minimum magnitude are indicated, the contour value with the maximum magnitude is 0.2, and the contour interval is 0.01 for all plots. The bold, dashed and thin contours are the ellipsoidal, γ_e, non-ellipsoidal, γ_n, and turning point, γ_c, strain values respectively.

unity are the most resilient, a result which compares well with the findings of Reinaud *et al.* (2003).

4.2. *Like-signed interactions ($\beta \geqslant 1$)*

We next turn to the general stability of like-signed vortices. In figure 7 we show contour maps of the turning-point strain rate $\gamma_c(\beta, \theta)$ for various height-to-width aspect ratios. The contour interval is 0.005 and the minimum and maximum values plotted are 0.005 and 0.2. The minimum strain contours appear on the right of the plots and increase to the left. As was seen for opposite-signed vortices the strain values increase as β approaches 1. One striking feature of like-signed vortices is that there appear to be no instabilities before the turning point, i.e. the margin of stability

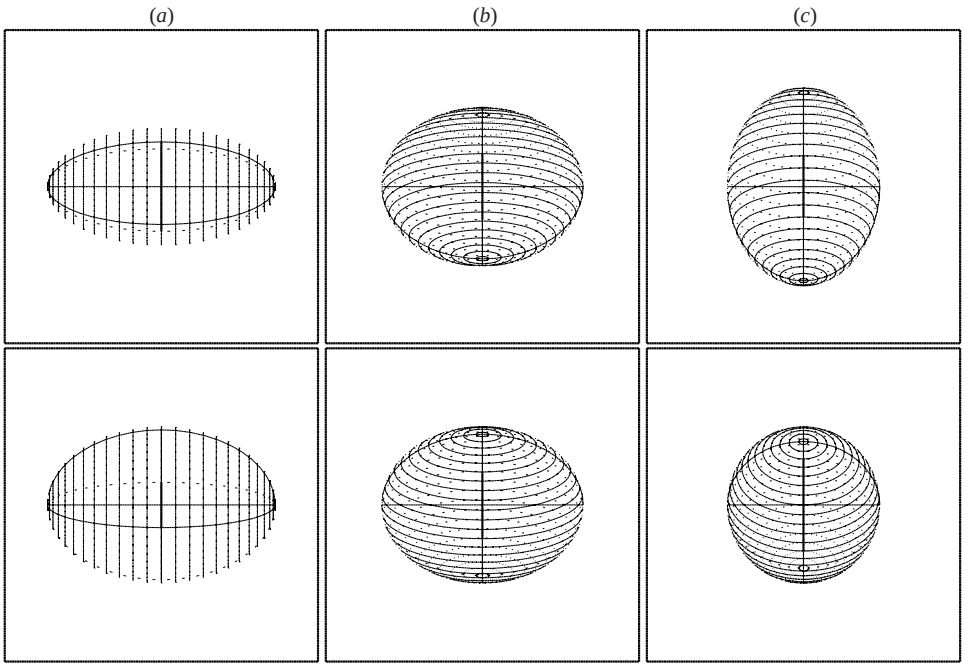

FIGURE 6. The ellipsoidal steady states at the turning point for $h/r = 1.0$, $\beta = -2$ and (*a*) $\theta = 30°$, (*b*) $\theta = 45.5°$ and (*c*) $\theta = 60°$. The images in the top row are projected onto the x-y plane, the images in the bottom row are projected onto the x-z plane.

coincides with the turning point, $\gamma_m = \gamma_c$. In fact, for $h/r \geqslant 1$, there is a marginal ellipsoidal instability before the turning point for $\theta = 0°$. However, this instability, which starts from $\sigma_r = \sigma_i = 0$, suggests the existence of a nearby branch of solutions with $\chi > 0$. The beginning of this branch in fact corresponds to a turning point in the solutions for $\theta > 0$, a turning point which occurs well before that found for θ precisely zero. Since in general vortex interactions are very unlikely to have θ precisely zero, we do not consider this exceptional case further.

From figure 7 we can also identify how the marginal strain γ_m varies with the angle θ. For $h/r < 0.8$, γ_m increases with increasing θ, but for $h/r \geqslant 0.8$ (as seen in the troughs in the curves as a function of θ) γ decreases for a range of θ values, before eventually reaching a maximum as $\theta \to 90°$. For $h/r \geqslant 0.8$ the minimum γ_m occurs for θ between 20° and 30°, i.e. at these angles vortices are least resilient to the background strain.

Again from the contour plots, we find that the greatest strain values occur for vortices with aspect ratio near 0.8, in agreement with the findings of Reinaud *et al.* (2003). Vortices with this aspect ratio are most resilient overall.

5. Conclusions

In this study, we have conducted a full linear stability analysis, using two methods: one for general disturbances and one for ellipsoidal disturbances. Over nearly the entire parameter space examined we found that the ellipsoidal steady states are stable, and where instability does occur the dominant modes encountered are ellipsoidal. Thus the ellipsoidal vortex in a linear background flow is a fairly robust model. The

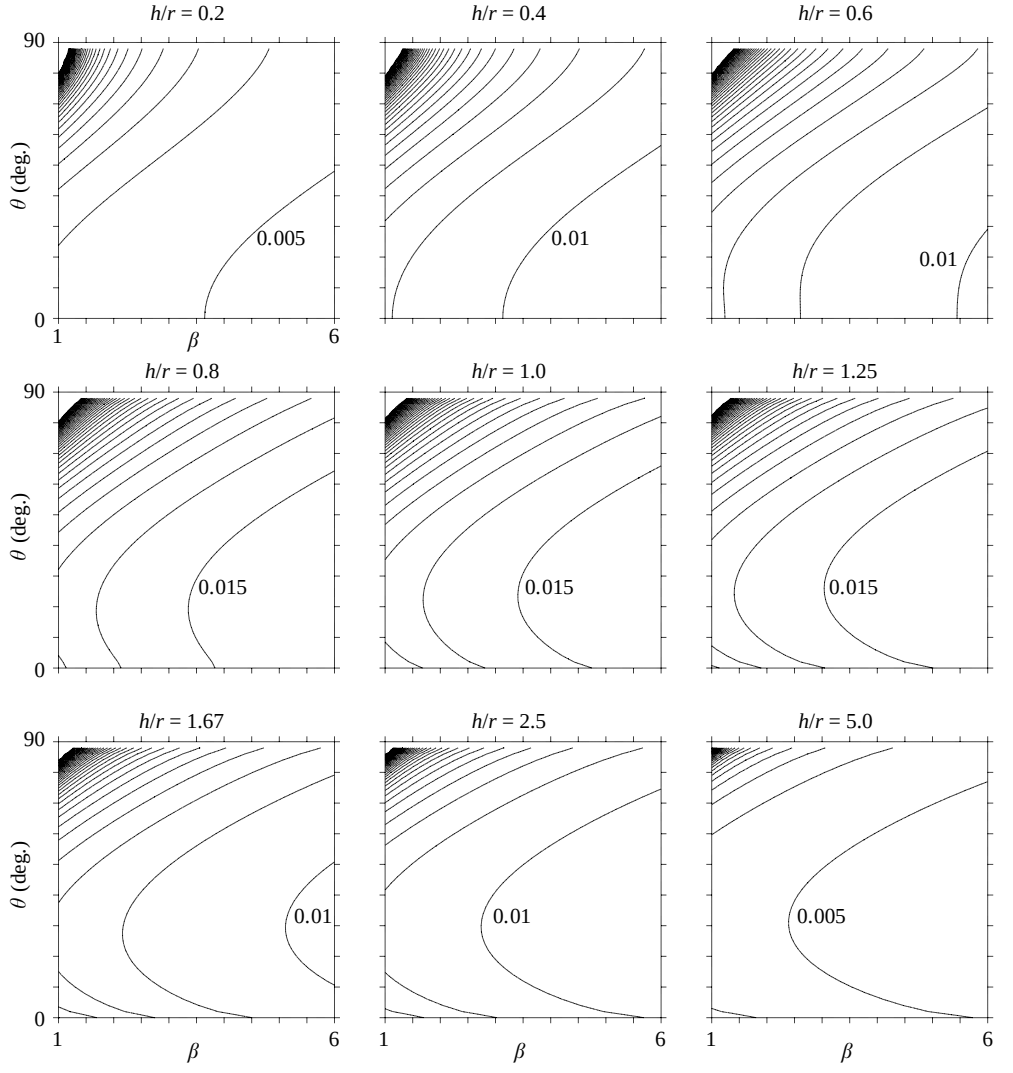

FIGURE 7. Contour maps of $\gamma_c(\beta,\theta)=\gamma_m(\beta,\theta)$ for various aspect ratios h/r for like-signed vortices ($\beta \geqslant 1$). The minimum contour values are indicated, the maximum contour value is 0.2, and the contour interval is 0.005 for all plots.

very few dominant non-ellipsoidal modes occur for opposite-signed prolate vortices with β near 0.8 and θ between 56° and 70°.

We also found that for vortices with aspect ratios greater than 0.8, the most unstable vortices (i.e. the ones which destabilize at the smallest γ_m values) are found in the ranges $55^\circ \leqslant \theta \leqslant 75^\circ$ and $20^\circ \leqslant \theta \leqslant 30^\circ$, for opposite- and like-signed vortices respectively. Because the strain is proportional to the inverse cube of the separation distances between two vortices, this implies that vortices which are vertically offset by these θ values destabilize from the greatest separation distances, i.e. they are least resilient. This agrees with the findings of Reinaud & Dritschel (2002) in which they examined the merger of two identical uniform-PV vortices which are offset both horizontally and vertically. They found that vortices which are moderately offset in the vertical merge from a greater separation distance than vortices not offset vertically.

For opposite-signed vortices we found that the most stable vortices have an aspect ratio between 1.0 and 1.25, whereas for the like-signed vortices the most stable vortices have an aspect ratio near 0.8 as was found by Reinaud *et al.* (2003).

The magnitude of the marginal strain increases as β approaches 1 for both opposite- and like-signed vortices. Thus this is the most stable value of β and implies that vortex interactions between vortices of greatly different sizes are least destructive, a result which is observed in QG turbulence (Reinaud *et al.* 2003).

In this work we were able to solve for the ellipsoidal modes analytically using the simple ellipsoid evolution equation. Interestingly the eigenmodes for this order correspond to the shape matrix, $\mathscr{B}$, whose components are proportional to the second-order moments of the ellipsoid. One can speculate that the eigenmodes at any order, m, are similarly related to the mth-order moments which are induced by perturbations of that order. If this is the case then by determining how these general perturbations evolve one could then use an approach like that used here for the ellipsoidal mode to solve analytically the general stability problem for the ellipsoid.

Appendix A. Elliptical integrals

Let

$$\Delta = \sqrt{(t+\alpha)(t+\beta)(t+\gamma)} \tag{A 1}$$

where α, β and γ are positive constants. The elliptical integral of the first kind is

$$R_F(\alpha, \beta, \gamma) = \frac{1}{2}\int_0^\infty \frac{\mathrm{d}t}{\Delta}. \tag{A 2}$$

Differentiation with respect to α, β and γ generates the elliptical integrals of the second kind:

$$R_D(\beta, \gamma, \alpha) = -6\frac{\partial R_F}{\partial \alpha} = \frac{3}{2}\int_0^\infty \frac{\mathrm{d}t}{(t+\alpha)\Delta} \tag{A 3a}$$

$$R_D(\gamma, \alpha, \beta) = -6\frac{\partial R_F}{\partial \beta} = \frac{3}{2}\int_0^\infty \frac{\mathrm{d}t}{(t+\beta)\Delta} \tag{A 3b}$$

$$R_D(\alpha, \beta, \gamma) = -6\frac{\partial R_F}{\partial \gamma} = \frac{3}{2}\int_0^\infty \frac{\mathrm{d}t}{(t+\gamma)\Delta}. \tag{A 3c}$$

From the above expressions, and using $\mathrm{d}(t/\Delta) = \mathrm{d}t/\Delta - t\mathrm{d}\Delta/\Delta^2$ together with

$$\mathrm{d}\Delta = \frac{1}{2}\Delta\left(\frac{1}{t+\alpha} + \frac{1}{t+\beta} + \frac{1}{t+\gamma}\right)\mathrm{d}t, \tag{A 4}$$

it is straightforward to show that

$$\alpha R_D(\beta, \gamma, \alpha) + \beta R_D(\gamma, \alpha, \beta) + \gamma R_D(\alpha, \beta, \gamma) = 3R_F(\alpha, \beta, \gamma). \tag{A 5}$$

The derivatives of the elliptical integrals of the second kind yield

$$\frac{\partial R_D(\beta, \gamma, \alpha)}{\partial \alpha} = -\frac{9}{4}\int_0^\infty \frac{\mathrm{d}t}{(t+\alpha)^2\Delta}, \tag{A 6a}$$

$$\frac{\partial R_D(\gamma, \alpha, \beta)}{\partial \beta} = -\frac{9}{4}\int_0^\infty \frac{\mathrm{d}t}{(t+\beta)^2\Delta}, \tag{A 6b}$$

$$\frac{\partial R_D(\alpha, \beta, \gamma)}{\partial \gamma} = -\frac{9}{4}\int_0^\infty \frac{\mathrm{d}t}{(t+\gamma)^2\Delta}, \tag{A 6c}$$

$$\frac{\partial R_D(\gamma,\alpha,\beta)}{\partial\alpha} = \frac{\partial R_D(\beta,\gamma,\alpha)}{\partial\beta} = -\frac{3}{4}\int_0^\infty \frac{\mathrm{d}t}{(t+\alpha)(t+\beta)\Delta}, \tag{A 6d}$$

$$\frac{\partial R_D(\beta,\gamma,\alpha)}{\partial\gamma} = \frac{\partial R_D(\alpha,\beta,\gamma)}{\partial\alpha} = -\frac{3}{4}\int_0^\infty \frac{\mathrm{d}t}{(t+\alpha)(t+\gamma)\Delta}, \tag{A 6e}$$

$$\frac{\partial R_D(\alpha,\beta,\gamma)}{\partial\beta} = \frac{\partial R_D(\gamma,\alpha,\beta)}{\partial\gamma} = -\frac{3}{4}\int_0^\infty \frac{\mathrm{d}t}{(t+\beta)(t+\gamma)\Delta}. \tag{A 6f}$$

Taking the derivative of (A 5) with respect to α, β and γ we obtain

$$\frac{\partial R_D(\beta,\gamma,\alpha)}{\partial\alpha} = -\frac{1}{\alpha}\left(\frac{3}{2}R_D(\beta,\gamma,\alpha) + \beta\frac{\partial R_D(\gamma,\alpha,\beta)}{\partial\alpha} + \gamma\frac{\partial R_D(\alpha,\beta,\gamma)}{\partial\alpha}\right), \tag{A 7a}$$

$$\frac{\partial R_D(\gamma,\alpha,\beta)}{\partial\beta} = -\frac{1}{\beta}\left(\frac{3}{2}R_D(\gamma,\alpha,\beta) + \alpha\frac{\partial R_D(\beta,\gamma,\alpha)}{\partial\beta} + \gamma\frac{\partial R_D(\alpha,\beta,\gamma)}{\partial\beta}\right), \tag{A 7b}$$

$$\frac{\partial R_D(\alpha,\beta,\gamma)}{\partial\gamma} = -\frac{1}{\gamma}\left(\frac{3}{2}R_D(\alpha,\beta,\gamma) + \alpha\frac{\partial R_D(\beta,\gamma,\alpha)}{\partial\gamma} + \beta\frac{\partial R_D(\gamma,\alpha,\beta)}{\partial\gamma}\right). \tag{A 7c}$$

Hence there are only three independent derivatives of the elliptical integrals of the second kind, i.e. $\partial R_D(\gamma,\alpha,\beta)/\partial\alpha$, $\partial R_D(\beta,\gamma,\alpha)/\partial\gamma$ and $\partial R_D(\alpha,\beta,\gamma)/\partial\beta$.

Considering $\partial R_D(\gamma,\alpha,\beta)/\partial\alpha$ only (since $\partial R_D(\beta,\gamma,\alpha)/\partial\gamma$ and $\partial R_D(\alpha,\beta,\gamma)/\partial\beta$ can be deduced by cyclic symmetry), there are four different cases. For the case $\alpha \neq \beta$ we can write

$$\frac{1}{(t+\alpha)(t+\beta)} = -\frac{1}{\alpha-\beta}\left(\frac{1}{t+\alpha} - \frac{1}{t+\beta}\right). \tag{A 8}$$

Using this we can write

$$\frac{\partial R_D(\gamma,\alpha,\beta)}{\partial\alpha} = \frac{1}{2(\alpha-\beta)}\left[R_D(\beta,\gamma,\alpha) - R_D(\gamma,\alpha,\beta)\right]. \tag{A 9}$$

If $\alpha = \beta < \gamma$ we cannot use the above formula but the integral becomes

$$\frac{\partial R_D(\gamma,\alpha,\beta)}{\partial\alpha} = -\frac{3}{4}\int_0^\infty \frac{\mathrm{d}t}{(t+\alpha)^3\sqrt{(t+\gamma)}} = \mathscr{I}_1 \tag{A 10}$$

where the solution $\mathscr{I}_1$ is given by (Abramowitz & Stegun 1965)

$$\mathscr{I}_1 = \frac{3}{8(\gamma-\alpha)^{\frac{5}{2}}}\ln\left[1 + \frac{\sqrt{\gamma-\alpha}}{\alpha}(\gamma+\sqrt{\gamma-\alpha})\right] + \frac{(2\gamma-5\alpha)\sqrt{\gamma}}{4\alpha^2(\alpha-\gamma)^2}. \tag{A 11}$$

If $\alpha < \beta = \gamma$ then the solution is

$$\frac{\partial R_D(\gamma,\alpha,\beta)}{\partial\alpha} = \mathscr{I}_2 \tag{A 12}$$

where $\mathscr{I}_2$ (Abramowitz & Stegun 1965) is

$$\mathscr{I}_2 = \frac{3}{8(\gamma-\alpha)^{\frac{5}{2}}}\left[\frac{\pi}{2} - \sin^{-1}\left(\frac{2\alpha}{\gamma} - 1\right)\right] - \frac{(\gamma-2\alpha)\sqrt{\alpha}}{4\gamma^2(\gamma-\alpha)^2}. \tag{A 13}$$

If $\alpha = \beta = \gamma$ then

$$\frac{\partial R_D(\gamma,\alpha,\beta)}{\partial\alpha} = \frac{\partial R_D(\beta,\gamma,\alpha)}{\partial\gamma} = \frac{\partial R_D(\alpha,\beta,\gamma)}{\partial\beta} = -\frac{3}{4}\int_0^\infty \frac{\mathrm{d}t}{(t+\alpha)^{7/2}} = \frac{3}{10}\alpha^{-5/2}. \tag{A 14}$$

Appendix B. Derivative of the self-induced flow matrix

Here we show how to determine the derivative of the self-induced flow matrix $\mathscr{S}_{\mathrm{v}} = \mathscr{L}\mathscr{P}_{\mathrm{v}}$ with respect to the elements of the matrix $\mathscr{B}$. As $\mathscr{L}$ is a constant matrix we only need to determine the derivative of the symmetric matrix $\mathscr{P}_{\mathrm{v}}$ which can be written as

$$\mathscr{P}_{\mathrm{v}} = \xi_a \hat{\boldsymbol{a}}\hat{\boldsymbol{a}}^T + \xi_b \hat{\boldsymbol{b}}\hat{\boldsymbol{b}}^T + \xi_c \hat{\boldsymbol{c}}\hat{\boldsymbol{c}}^T \tag{B 1}$$

where $\hat{\boldsymbol{a}}$, $\hat{\boldsymbol{b}}$, $\hat{\boldsymbol{c}}$ are the unit vectors along the ellipsoid axes and ξ_a, ξ_b, ξ_c are given in terms of the elliptical integrals of the second kind as follows:

$$\xi_a = \kappa_v R_D(b^2, c^2, a^2), \qquad \xi_b = \kappa_v R_D(c^2, a^2, b^2), \qquad \xi_c = \kappa_v R_D(a^2, b^2, c^2), \tag{B 2}$$

where κ_v is the vortex strength. Taking the derivative of (B 1) with respect to the $\mathscr{B}$ matrix elements B^k gives

$$\begin{aligned}\frac{\partial \mathscr{P}_{\mathrm{v}}}{\partial B^k} = {} & \frac{\partial \xi_a}{\partial B^k}\hat{\boldsymbol{a}}\hat{\boldsymbol{a}}^T + \xi_a \frac{\partial \hat{\boldsymbol{a}}}{\partial B^k}\hat{\boldsymbol{a}}^T + \xi_a \hat{\boldsymbol{a}}\frac{\partial \hat{\boldsymbol{a}}^T}{\partial B^k} + \frac{\partial \xi_b}{\partial B^k}\hat{\boldsymbol{b}}\hat{\boldsymbol{b}}^T + \xi_b \frac{\partial \hat{\boldsymbol{b}}}{\partial B^k}\hat{\boldsymbol{b}}^T \\ & + \xi_b \hat{\boldsymbol{b}}\frac{\partial \hat{\boldsymbol{b}}^T}{\partial B^k} + \frac{\partial \xi_c}{\partial B^k}\hat{\boldsymbol{c}}\hat{\boldsymbol{c}}^T + \xi_c \frac{\partial \hat{\boldsymbol{c}}}{\partial B^k}\hat{\boldsymbol{c}}^T + \xi_c \hat{\boldsymbol{c}}\frac{\partial \hat{\boldsymbol{c}}^T}{\partial B^k}. \end{aligned} \tag{B 3}$$

Now, since $\partial \mathscr{B}/\partial B^k = \mathscr{J}^k$, and using the eigen-relations $\mathscr{B}\hat{\boldsymbol{a}} = a^2\hat{\boldsymbol{a}}$, etc., together with the complementary relations $\hat{\boldsymbol{a}}^T\mathscr{B} = a^2\hat{\boldsymbol{a}}^T$, where $\hat{\boldsymbol{a}}$, $\hat{\boldsymbol{b}}$ and $\hat{\boldsymbol{c}}$ are orthonormal vectors, we find

$$\frac{\partial a^2}{\partial B^k} = \hat{\boldsymbol{a}}^T \mathscr{J}^k \hat{\boldsymbol{a}}, \qquad \frac{\partial b^2}{\partial B^k} = \hat{\boldsymbol{b}}^T \mathscr{J}^k \hat{\boldsymbol{b}}, \qquad \frac{\partial c^2}{\partial B^k} = \hat{\boldsymbol{c}}^T \mathscr{J}^k \hat{\boldsymbol{c}}. \tag{B 4}$$

The derivatives of the unit vectors, like the derivatives of the squared axis lengths, are obtained by differentiating the eigen-relations $\mathscr{B}\hat{\boldsymbol{a}} = a^2\hat{\boldsymbol{a}}$, etc., giving

$$\mathscr{J}^k\hat{\boldsymbol{a}} + \mathscr{B}\frac{\partial \hat{\boldsymbol{a}}}{\partial B^k} = \frac{\partial a^2}{\partial B^k}\hat{\boldsymbol{a}} + a^2\frac{\partial \hat{\boldsymbol{a}}}{\partial B^k}, \tag{B 5a}$$

$$\mathscr{J}^k\hat{\boldsymbol{b}} + \mathscr{B}\frac{\partial \hat{\boldsymbol{b}}}{\partial B^k} = \frac{\partial b^2}{\partial B^k}\hat{\boldsymbol{b}} + b^2\frac{\partial \hat{\boldsymbol{b}}}{\partial B^k}, \tag{B 5b}$$

$$\mathscr{J}^k\hat{\boldsymbol{c}} + \mathscr{B}\frac{\partial \hat{\boldsymbol{c}}}{\partial B^k} = \frac{\partial c^2}{\partial B^k}\hat{\boldsymbol{c}} + c^2\frac{\partial \hat{\boldsymbol{c}}}{\partial B^k}. \tag{B 5c}$$

Left multiplying (B 5*a*) by $\hat{\boldsymbol{b}}^T$ and $\hat{\boldsymbol{c}}^T$, (B 5*b*) by $\hat{\boldsymbol{a}}^T$ and $\hat{\boldsymbol{c}}^T$, and (B 5*c*) by $\hat{\boldsymbol{a}}^T$ and $\hat{\boldsymbol{b}}^T$, we obtain

$$\hat{\boldsymbol{b}}^T\mathscr{J}^k\hat{\boldsymbol{a}} = (a^2 - b^2)\hat{\boldsymbol{b}}^T\frac{\partial \hat{\boldsymbol{a}}}{\partial B^k}, \qquad \hat{\boldsymbol{c}}^T\mathscr{J}^k\hat{\boldsymbol{a}} = (a^2 - c^2)\hat{\boldsymbol{c}}^T\frac{\partial \hat{\boldsymbol{a}}}{\partial B^k}, \tag{B 6a}$$

$$\hat{\boldsymbol{a}}^T\mathscr{J}^k\hat{\boldsymbol{b}} = (b^2 - a^2)\hat{\boldsymbol{a}}^T\frac{\partial \hat{\boldsymbol{b}}}{\partial B^k}, \qquad \hat{\boldsymbol{c}}^T\mathscr{J}^k\hat{\boldsymbol{b}} = (b^2 - c^2)\hat{\boldsymbol{c}}^T\frac{\partial \hat{\boldsymbol{b}}}{\partial B^k}, \tag{B 6b}$$

$$\hat{\boldsymbol{a}}^T\mathscr{J}^k\hat{\boldsymbol{c}} = (c^2 - a^2)\hat{\boldsymbol{a}}^T\frac{\partial \hat{\boldsymbol{c}}}{\partial B^k}, \qquad \hat{\boldsymbol{b}}^T\mathscr{J}^k\hat{\boldsymbol{c}} = (c^2 - b^2)\hat{\boldsymbol{b}}^T\frac{\partial \hat{\boldsymbol{c}}}{\partial B^k}. \tag{B 6c}$$

Since $\hat{\boldsymbol{a}}$, $\hat{\boldsymbol{b}}$ and $\hat{\boldsymbol{c}}$ are unit vectors, their derivatives are perpendicular to them. Hence, the above equations are sufficient to determine the required derivatives:

$$\frac{\partial \hat{\boldsymbol{a}}}{\partial B^k} = \lambda^k_{ab}\hat{\boldsymbol{b}} - \lambda^k_{ca}\hat{\boldsymbol{c}}, \qquad \frac{\partial \hat{\boldsymbol{b}}}{\partial B^k} = \lambda^k_{bc}\hat{\boldsymbol{c}} - \lambda^k_{ab}\hat{\boldsymbol{a}}, \qquad \frac{\partial \hat{\boldsymbol{c}}}{\partial B^k} = \lambda^k_{ca}\hat{\boldsymbol{a}} - \lambda^k_{bc}\hat{\boldsymbol{b}}, \tag{B 7a–c}$$

where we have the following scalars:

$$\lambda_{ab}^k = \frac{\hat{\boldsymbol{a}}^T \mathscr{J}^k \hat{\boldsymbol{b}}}{a^2 - b^2}, \quad \lambda_{bc}^k = \frac{\hat{\boldsymbol{b}}^T \mathscr{J}^k \hat{\boldsymbol{c}}}{b^2 - c^2}, \quad \lambda_{ca}^k = \frac{\hat{\boldsymbol{c}}^T \mathscr{J}^k \hat{\boldsymbol{a}}}{c^2 - a^2}. \tag{B 8a–c}$$

The derivatives of ξ_a, ξ_b and ξ_c are

$$\frac{\partial \xi_a}{\partial B^k} = \frac{\partial a^2}{\partial B^k}\frac{\partial \xi_a}{\partial a^2} + \frac{\partial b^2}{\partial B^k}\frac{\partial \xi_a}{\partial b^2} + \frac{\partial c^2}{\partial B^k}\frac{\partial \xi_a}{\partial c^2}, \tag{B 9a}$$

$$\frac{\partial \xi_b}{\partial B^k} = \frac{\partial a^2}{\partial B^k}\frac{\partial \xi_b}{\partial a^2} + \frac{\partial b^2}{\partial B^k}\frac{\partial \xi_b}{\partial b^2} + \frac{\partial c^2}{\partial B^k}\frac{\partial \xi_b}{\partial c^2}, \tag{B 9b}$$

$$\frac{\partial \xi_c}{\partial B^k} = \frac{\partial a^2}{\partial B^k}\frac{\partial \xi_c}{\partial a^2} + \frac{\partial b^2}{\partial B^k}\frac{\partial \xi_c}{\partial b^2} + \frac{\partial c^2}{\partial B^k}\frac{\partial \xi_c}{\partial c^2}, \tag{B 9c}$$

where the derivatives of the squared axis lengths are given by (B 4) and the derivatives of ξ_a, etc. are obtained using derivatives of the elliptical integrals given in Appendix A and derivatives of the vortex strength, κ_v, i.e.

$$\frac{\partial \kappa_v}{\partial a^2} = \frac{\kappa_v}{2a^2}, \quad \frac{\partial \kappa_v}{\partial b^2} = \frac{\kappa_v}{2b^2}, \quad \frac{\partial \kappa_v}{\partial c^2} = \frac{\kappa_v}{2c^2}. \tag{B 10}$$

Finally using (B 4), (B 7) and (B 9) in (B 3) gives

$$\frac{\partial \mathscr{P}_{\mathrm{v}}}{\partial B^k} = \mathscr{M}\mathscr{Q}^k\mathscr{M}^T \tag{B 11}$$

where $\mathscr{M}$ is the matrix whose columns are the unit vectors $\hat{\boldsymbol{a}}$, $\hat{\boldsymbol{b}}$ and $\hat{\boldsymbol{c}}$, and the matrices $\mathscr{Q}^k$, $k = 1, \ldots, 5$, are defined as follows:

$$\mathscr{Q}^k = \begin{pmatrix} \dfrac{\partial \xi_a}{\partial B^k} & \lambda_{ab}^k(\xi_a - \xi_b) & \lambda_{ca}^k(\xi_c - \xi_a) \\ \lambda_{ab}^k(\xi_a - \xi_b) & \dfrac{\partial \xi_b}{\partial B^k} & \lambda_{bc}^k(\xi_b - \xi_c) \\ \lambda_{ca}^k(\xi_c - \xi_a) & \lambda_{bc}^k(\xi_b - \xi_c) & \dfrac{\partial \xi_c}{\partial B^k} \end{pmatrix}. \tag{B 12}$$

This form for the matrices $\mathscr{Q}^k$ is singular when two of the axis lengths are equal. However using (A 8), (A 9) and (B 10) one can show that

$$\lambda_{ab}^k(\xi_a - \xi_b) = \hat{\boldsymbol{a}}^T \mathscr{J}^k \hat{\boldsymbol{b}} \left(2\frac{\partial \xi_a}{\partial b^2} - \frac{\xi_a}{b^2} \right), \tag{B 13a}$$

$$\lambda_{bc}^k(\xi_b - \xi_c) = \hat{\boldsymbol{b}}^T \mathscr{J}^k \hat{\boldsymbol{c}} \left(2\frac{\partial \xi_b}{\partial c^2} - \frac{\xi_b}{c^2} \right), \tag{B 13b}$$

$$\lambda_{ca}^k(\xi_c - \xi_a) = \hat{\boldsymbol{c}}^T \mathscr{J}^k \hat{\boldsymbol{a}} \left(2\frac{\partial \xi_c}{\partial a^2} - \frac{\xi_c}{a^2} \right). \tag{B 13c}$$

As the derivatives of ξ_a, ξ_b and ξ_c can be evaluated for all values of a, b and c (see Appendix A) we can thus determine the $\mathscr{Q}^k$ matrices.

REFERENCES

Abramowitz, M. & Stegun, I. A. 1965 *Handbook of Mathematical Functions*. Dover.

Armi, L., Herbert, D., Oakey, N., Price, J., Richardson, P., Rossby, T. & Ruddick, B. 1989 Two years in the life of a mediterranean salt lens. *J. Phys. Oceanogr.* **19**, 354–370.

Dritschel, D. G. 1990 The stability of elliptical vortices in an external straining flow. *J. Fluid Mech.* **210**, 223–261, 1990.

Dritschel, D. G., Scott, R. K. & Reinaud, J. N. 2005 The stability of quasi-geostrophic ellipsoidal vortices. *J. Fluid Mech.* **536**, 401–421.

Ebbesmeyer, C. C., Taft, B. A., McWilliams, J. C., Shen, C. Y., Riser, S. C., Rossby, H. T., Biscaye, P. E. & Östlund, H. G. 1986 Detection, structure, and origin of extreme anomalies in a Western Atlantic oceanographic section. *J. Phys. Oceanogr.* **16**, 591–612.

Hashimoto, H., Shimonishi, T. & Miyazaki, T. 1999 Quasigeostrophic ellipsoidal vortices in a two-dimensional strain field. *J. Phys. Soc Japan* **68**, 3863–3880.

Holton, J. R., Haynes, P. H., McIntyre, M. E., Douglass, A. R., Rood, R. B. & Pfister, L. 1995 Stratosphere-troposphere exchange field. *Revs. Geophys.* **33**, 403–439.

Kida, S. 1981 Motion of an elliptical vortex in a uniform shear flow. *J. Phys. Soc Japan* **50**, 3517–3520.

Laplace, P. S. 1784 *Théorie du Mouvement et de la Figure Elliptique des Planetès.* Imprimerie de Ph.-D. Pierres, Paris, 153 pp.

McKiver, W. J. & Dritschel, D. G. 2003 The motion of a fluid ellipsoid in a general linear background flow. *J. Fluid Mech.* **474**, 147–173.

Meacham, S. P. 1992 Quasigeostrophic, ellipsoidal vortices in a stratified fluid. *Dyn. Atmos. Oceans* **16**, 189–223.

Meacham, S. P., Pankratov, K. K., Shchepetkin, A. F. & Zhmur, V. V. 1994 The interaction of ellipsoidal vortices with background shear flows in a stratified fluid. *Dyn. Atmos. Oceans* **21**, 167–212.

Miyazaki, T., Ueno, K. & Shimonishi, T. 1999 Quasigeostrophic tilted spheroidal vortices. *J. Phys. Soc Japan* **68**, 2592–2601.

Miyazaki, T., Furuichi, Y. & Takahashi, N. 2001 Quasigeostrophic ellipsoidal vortex model. *J. Phys. Soc Japan* **70**, 1942–1953.

Reinaud, J. & Dritschel, D. G. 2002 The merger of vertically offset quasi-geostrophic vortices. *J. Fluid Mech.* **469**, 287–315.

Reinaud, J., Dritschel, D. G. & Koudella, C. R. 2003 The shape of vortices in quasi-geostrophic turbulence. *J. Fluid Mech.* **474**, 175–191.

Zhmur, V. V. & Shchepetkin, A. F. 1991 Evolution of an ellipsoidal vortex in a stratified ocean: survivability of the vortex in flow with vertical shear. *Izv. AN SSSR Phys. Atmos. Ocean* **27(5)**, 492–503.